Oligomerization-Induced Differential Dephosphorylation of c-Met Receptor Tyrosine Kinase†

Payal R. Sheth and Stanley J. Watowich*

Department of Human Biological Chemistry and Genetics and Sealy Center for Structural Biology, University of Texas Medical Branch, Galveston, Texas 77555-0645

Received May 9, 2005; Revised Manuscript Received June 21, 2005

ABSTRACT: Although protein tyrosine phosphatases (PTPs) are significant negative regulators of receptor tyrosine kinase (RTK)-initiated cell signaling, it is unknown how RTK oligomerization modulates the equilibrium established between kinase and phosphatase activity. To determine the impact of oligomerization on the ability of c-MET RTK to undergo dephosphorylation, we examined the relative dephosphorylation kinetics of similarly phosphorylated dimeric TPR-MET and monomeric cytoMET. Notably, we observed that the dephosphorylation kinetics of phosphorylated MET were significantly modulated by its oligomeric state, with the global dephosphorylation rate of TPR-MET severalfold slower than the dephosphorylation rate of monomeric cytoMET. Furthermore, there were important site-specific differences in the dephosphorylation patterns of cytoMET and TPR-MET. Reduced dephosphorylation activity was predicted to eliminate or reduce the requirement of ligand-dependent oligomerization for MET autophosphorylation. This was demonstrated by the rapid phosphorylation of unstimulated c-MET on its activation loop and carboxy-terminal tyrosines following pervanadate treatment of cells expressing c-MET. We conclude that the MET oligomerization state is a critical regulator of its dephosphorylation rate. Thus, oligomerization plays a role in modifying the receptor's kinase and dephosphorylation rates to change the equilibrium levels of phosphorylated and dephosphorylated receptor in response to ligand stimulation, and that this may be a general mechanism utilized by many oligomeric receptor tyrosine kinases for regulation of their activity.

Although receptor tyrosine kinases (RTKs)[1] are major activators of intracellular signaling pathways that promote cellular proliferation, differentiation, migration, and motility, the detailed molecular mechanisms responsible for RTK activation are largely unknown (*1*−*3*). RTK signaling typically involves a progression of events that include binding of a cognate ligand to a receptor's extracellular domain, subsequent receptor dimerization (or higher-order oligomerization), and autophosphorylation of selected tyrosine residues located within the receptor's cytoplasmic domain. These phosphotyrosines serve as docking sites for effector molecules that propagate RTK-initiated intracellular signals. RTK activity is downregulated or modulated by several mechanisms, including receptor dephosphorylation, endocytosis, and degradation (*1*, *2*, *4*).

Recently, several studies have sought to provide deeper insights into the molecular mechanisms underlying RTK activation, signaling, and regulation. Although ligand-mediated receptor dimerization appears to be a common event preceding RTK activation, structures of several receptor ectodomains bound to their cognate ligands showed RTKs used different binding modes to induce dimerization (*5*−*7*).

Irrespective of the mode of dimerization, autophosphorylation of the RTK cytoplasmic domain typically occurs following dimerization. Autophosphorylation has repeatedly been shown to regulate the catalytic activity of RTKs, and create binding sites for effector molecule recruitment, although the mechanism whereby dimerization induces autophosphorylation is unknown. Kinase domain structures from the insulin receptor (IR), FGFR, and c-MET, complemented with biochemical data, have provided insights into possible molecular mechanisms of substrate phosphorylation and autophosphorylation (*8*−*16*). The correlation between ligand binding and increased levels of autophosphorylation and substrate phosphorylation have also been studied (*12*, *14*).

The importance of dephosphorylation in regulating RTK activation has been demonstrated by ligand-independent platelet-derived growth factor receptor (PDGFR) and IR autophosphorylation following pervanadate treatment in cultured cells (*17*, *18*). These studies implied that RTK phosphorylation was dynamically regulated by the combined action of kinase and phosphatase activity. A recent study

† This work was supported by Grant 4952-052 (S.J.W.) from the Texas Higher Education Coordinating Board and the Sealy Center for Structural Biology.

* To whom correspondence should be addressed: Department of Human Biological Chemistry and Genetics, University of Texas Medical Branch, Galveston, TX 77555-0645. Telephone: (409) 747-4749. Fax: (409) 747-4745. E-mail: watowich@xray.utmb.edu.

[1] Abbreviations: RTK, receptor tyrosine kinase; PTP, protein tyrosine phosphatase; PDGF, platelet-derived growth factor; EGF, epidermal growth factor; HGF, hepatocyte growth factor; FGF, fibroblast growth factor; VEGF, vascular endothelial growth factor; IR, insulin receptor; CIAP, calf alkaline phosphatase; CHAPS, 3-[(3-cholamidopropyl)-dimethylammonio]-1-propanesulfonic acid; PY, phosphotyrosine; Y, tyrosine.

10.1021/bi050855u CCC: $30.25
Published on Web 07/26/2005

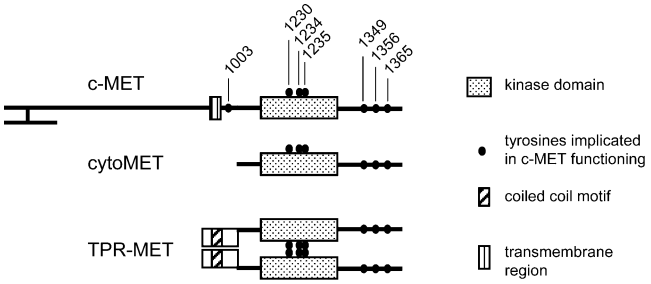

FIGURE 1: Domain organization of c-MET, cytoMET, and TPR-MET. CytoMET corresponds to the cytoplasmic portion of c-MET contained within TPR-MET. TPR-MET corresponds to a fusion between the cytoplasmic domain of c-MET and TPR, a coiled-coil domain from the nuclear pore complex. The coiled-coil interactions within the TPR domain render TPR-MET a constitutive dimer (*24*). Tyrosines that have been implicated in c-MET functioning are marked. Both cytoMET and TPR-MET proteins contain all known phosphorylation sites within the activation loop (corresponding to c-MET Y^{1230}, Y^{1234}, and Y^{1235}) and the carboxy-terminal tail (corresponding to c-MET Y^{1349}, Y^{1356}, and Y^{1365}).

has suggested that oligomerization might modulate RTK dephosphorylation (*19*). Unfortunately, the chemical cross-linking step used in that study made it difficult to accurately correlate differences in dephosphorylation to a unique receptor oligomeric state, and cellular cofactors co-immunoprecipitating with different receptor oligomeric states may have also contributed to the observed differential dephosphorylation (*19*). Thus, although this work showed that ligand-activated PDGFR was resistant to dephosphorylation, the mechanism of resistance was largely unknown (*19*). In our current study, we examined if oligomerization alone was sufficient to induce resistance to dephosphorylation.

We have recently utilized a well-defined in vitro system, consisting of functional monomeric and dimeric forms of c-MET, to develop a detailed understanding of how oligomerization state modulates a receptor's biochemical and conformational properties and thus contributes to receptor activation (*20*, *21*). c-MET, the RTK for hepatocyte growth factor/scatter factor (HGF/SF), is responsible for cell proliferation, differentiation, branching morphogenesis, and protein synthesis associated with an invasive cell phenotype (*22*). Sustained c-MET signaling, caused by c-MET overexpression, HGF overexpression, or activating c-MET mutations, has been linked to solid tumor growth and metastasis (*22*, *23*). TPR-MET, a naturally occurring oncoprotein resulting from fusion of the TPR region of the nuclear pore complex and the cytoplasmic domain of c-MET, recapitulated many of the molecular and cellular properties of ligand-activated c-MET (*24*, 25). Thus, it is an established model system for the ligand-dependent oligomeric state of c-MET (Figure 1). The isolated cytoplasmic domain of c-MET (cytoMET; Figure 1) served as a functional analogue of monomeric c-MET. Detailed comparative kinetic analysis of similarly phosphorylated TPR-MET and cytoMET showed that the RTK oligomeric state substantially influenced its kinetic and thermodynamic properties, implying that functionally necessary conformational changes accompanied receptor oligomerization (*20*, *21*).

Regulation of c-MET by protein tyrosine phosphatases (PTPs) is poorly understood, although studies using substrate trapping mutants, antisense RNA, and phosphotyrosine peptides have proposed DEP-1 (CD148/PTP-η), PTP-S, and leukocyte common antigen-related (LAR) to be potentially involved in c-MET regulation (*26*−*28*). Detailed animal model or cell culture studies have yet to substantiate a role of these indicated PTPs in c-MET signaling. Moreover, DEP-1 was observed to preferentially dephosphorylate carboxyl-terminal tyrosines Y^{1349} and Y^{1365} in c-MET, suggesting that phosphatase site-specific preferences might be an additional mechanism for regulating receptor signaling (*28*).

To better understand the relationship among RTK oligomerization, dephosphorylation, and receptor regulation, we present data showing the RTK dephosphorylation can be modulated by its oligomeric state. These studies used the well-behaved TPR-MET/cytoMET system to represent ligand-stimulated oligomeric and unactivated monomeric forms of c-MET (*20*, *21*, *24*) and demonstrated that oligomerization interfered with receptor dephosphorylation. Our results revealed a "protective" role for oligomerization in dephosphorylation of c-MET RTK, which could be crucial for proper activation and regulation of the receptor. Furthermore, our data suggest a dynamic flux balance exists between the kinase and phosphatase activities associated with RTKs, and when these fluxes are differentially perturbed by oligomerization, tyrosines necessary for RTK signaling are rapidly phosphorylated.

EXPERIMENTAL PROCEDURES

Cell Culture. Vero cells (African green monkey kidney cells) were obtained from the American Tissue Culture Collection. Cells were grown at 37 °C in 5% CO_2 and minimum essential medium (MEM) supplemented with glutamine and 5% FBS.

Materials and Reagents. c-Met anti-phospho $Y^{1234,1235}$, mouse monoclonal anti-phosphotyrosine clone 4G10, anti-MET DO-24, anti-MET DO-21, Protein A agarose, PTP1B, and recombinant PTPβ were obtained from Upstate Biotechnology, Inc. c-Met anti-phospho Y^{1349} and anti-phospho Y^{1365} were obtained from Cell Signaling Technology and Biosource International, respectively. Calf intestinal alkaline phosphatase (CIAP) was from Invitrogen Life Technologies (GIBCO). Anti-c-MET SC-161 was obtained from Santa Cruz Biotechnology. Anti-rabbit and anti-mouse HRP-linked conjugates were obtained from Southern Biotechnology Associates, Inc., and Amersham Biosciences, respectively. All other chemicals were from Sigma unless otherwise noted.

Protein Expression and Purification. TPR-MET and cytoMET (cytoplasmic domain of the c-MET receptor; Figure 1) expression and purification have been described previously (*21*). Briefly, both proteins were cloned into the Bac-to-Bac baculovirus expression system (Invitrogen) with a carboxy-terminal hexahistidine sequence. For expression, Sf-9 insect cells were infected with recombinant baculovirus, and cells were harvested 72 h post-infection and lysed in TBSC lysis buffer [50 mM Tris (pH 7.5), 150 mM NaCl, and 0.5% CHAPS] supplemented with 1 mM DTT and 1× Complete Protease Inhibitor Cocktail (Roche). TPR-MET and cytoMET were separately purified from the cleared lysate by binding and elution from Ni−NTA beads (Qiagen). Purified protein was dialyzed into PBSC [50 mM sodium phosphate (pH 6.5), 150 mM NaCl, 0.5% CHAPS, and 1 mM DTT] supplemented with 50 μM ATP, 25 mM $MgCl_2$, and 5 mM $MnCl_2$ to ensure complete autophosphorylation.

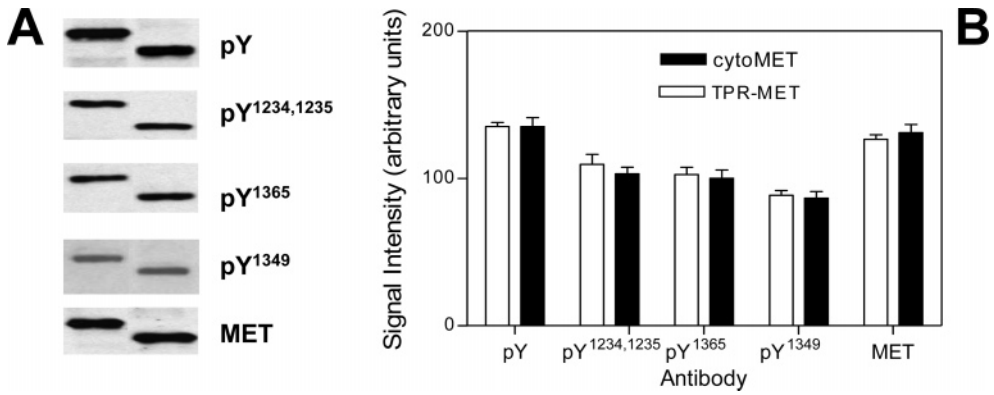

FIGURE 2: Phosphorylation levels in cytoMET and TPR-MET. The phosphorylation levels in cytoMET and TPR-MET were measured using different phospho-specific antibodies. Equimolar quantities of purified cytoMET and TPR-MET proteins were separated on polyacrylamide gels and subjected to Western blot analyses using anti-PY (4G10). The membranes were stripped and reprobed with anti-phospho $Y^{1234,1235}$, anti-phospho Y^{1349}, anti-phospho Y^{1365}, and anti-MET antibody as a loading control. The higher-molecular mass band corresponds to TPR-MET (~60 kDa), and the lower-molecular mass band corresponds to cytoMET (~40 kDa). X-ray films containing the protein bands were imaged in a MultiImage Light Cabinet (Alpha Innotech Corp.), and densitometry was performed using ChemiImager software provided by the manufacturer. Experiments were performed within the dynamic range of the antibody signal and the exposure time. The data from the densitometry analyses for cytoMET and TPR-MET are depicted as a bar graph in panel B. The data are presented as the mean of three different experiments with error bars representing standard deviations. Comparable levels of phosphorylation were seen at two different protein concentrations (data not shown).

Excess ATP, ADP, $MgCl_2$, and $MnCl_2$ were removed by successive dialysis against PBSC. The proteins were further purified via gel filtration column (Phenomenex BIOSEP SEC-3000 column) chromatography. Protein concentrations were determined by A_{280} with molar extinction coefficients calculated on the basis of the aromatic content of the proteins.

In Vitro Dephosphorylation Assay and Western Blot Analysis. Fixed concentrations of phosphorylated TPR-MET or cytoMET were separately incubated with recombinant PTPβ (2 units/μL final concentration) in the dephosphorylation reaction buffer [25 mM HEPES (pH 7.2), 50 mM NaCl, 5 mM dithiothreitol, and 2.5 mM EDTA] at 37 °C. At specified time points, reaction aliquots were removed and quenched in SDS−PAGE buffer. Proteins were separated on 10% polyacrylamide gels and transferred to a PVDF membrane using standard procedures. After incubation overnight in blocking buffer (1% BSA in TBST) at 4 °C, the membranes were incubated with phosphotyrosine-specific antibodies (typically at a 1:1000 dilution, except in anti-phospho $Y^{1234,1235}$ where a 1:500 dilution was used), washed in TBST, and incubated with HRP-coupled secondary antibody (1:10000 dilution). Antibodies were detected using an ECL Plus chemiluminescent kit (Amersham) and exposure to film (Kodak X-OMAT AR). Antibodies were removed from the membranes in stripping buffer [100 mM 2-mercaptoethanol and 2% SDS in 62.5 mM Tris-HCl (pH 6.7)] at 65 °C for 45 min, reblocked, and reprobed with anti-MET antibody. X-ray films containing the protein bands were imaged with a MultiImage Light Cabinet (Alpha Innotech Corp.), and densitometry was performed using ChemiImager software (Alpha Innotech Corp.). Experiments were performed within the dynamic range of the antibody signal and the exposure time. A similar protocol was used for dephosphorylation with PTP1B and CIAP. GraphPad Prism was used for data fitting and statistical analysis. Unless otherwise mentioned, all experiments were carried out in triplicate.

Pervanadate-Induced c-MET RTK Autophosphorylation. The cells were grown to confluency and serum starved for 12−24 h. Pervanadate was prepared by mixing 500 μL of 100 mM Na_3VO_4 with 500 μL of 100 mM H_2O_2 and incubating the mixture at room temperature for 20 min. The solution was cooled on ice and added to cell medium to yield a final concentration of 50 μM pervanadate as denoted by the vanadate concentration in the medium. Stimulation was carried out at room temperature with pervanadate-containing media, and at indicated time points, the cells were washed with ice-cold PBS and lysed in Triton X-100 lysis buffer [50 mM Tris (pH 7.5), 150 mM NaCl, 1% Triton X-100, 3 mM Na_3VO_4, 2 mM EDTA, 2 mM NaF, and protease inhibitor cocktail]. Protein concentrations in each lysate were determined using the Bio-Rad DC assay. Lysates containing 1 mg of protein were used for immunoprecipitation of c-MET with DO-24 antibody, which recognizes the c-MET extracellular region. Briefly, lysate was incubated with the antibody overnight at 4 °C, after which ~100 μL of Protein A agarose in PBS was added to the mixture for 3−4 h at 4 °C to capture the immune complex. The lysate and beads were centrifuged; the supernatant was removed, and beads were washed extensively in lysis buffer before being resuspended in SDS−PAGE buffer. Samples were separated on 7.5% polyacrylamide gels, and immunoblotting was performed as described above with blocking buffer (3% BSA in TBST).

RESULTS

TPR-MET and CytoMET Phosphorylation. Both TPR-MET (~60 kDa) and cytoMET (~44 kDa) were separately purified from Sf9 cells to >90% homogeneity (data not shown) (*21*). Previous studies showed that TPR-MET was dimeric in solution and cytoMET monomeric (*21*). Both proteins were shown to be phosphorylated and active as kinases in vitro (*21*). To test the relative phosphorylation levels of the proteins, quantitative Western blot analysis of purified TPR-MET and cytoMET using antibodies against phosphorylated tyrosines (4G10), activation loop $Y^{1234,1235}$, and carboxy-terminal tail Y^{1349} and Y^{1365} were performed. These analyses showed the same tyrosines on both proteins were phosphorylated to identical levels (Figure 2). Furthermore, incubation of phosphorylated TPR-MET or cytoMET with [γ-^{32}P]ATP revealed no further incorporation of phos-

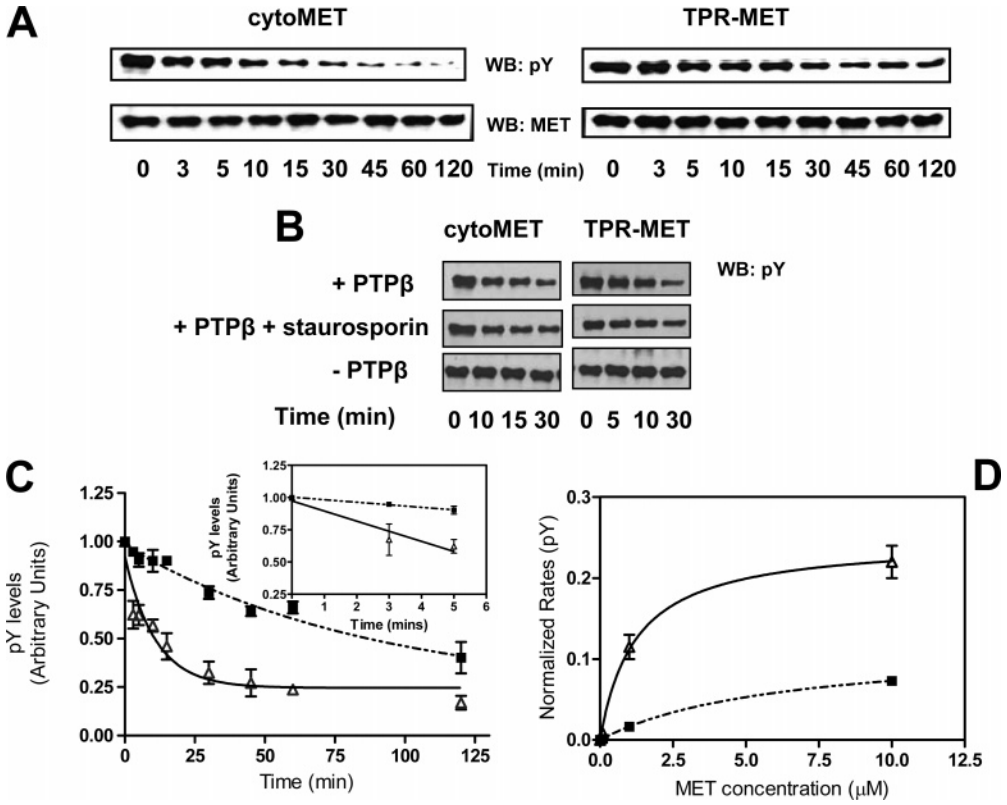

FIGURE 3: Global dephosphorylation in cytoMET and TPR-MET. Purified phosphorylated protein (1 μM) was incubated in phosphatase buffer with PTPβ, and aliquots were removed at the indicated times. The proteins were separated on polyacrylamide gels, transferred to a PVDF membrane, and probed with phosphotyrosine antibody. The blots were stripped and reprobed with anti-MET antibody. Control experiments were performed in the presence of staurosporine in the MET/PTPβ mixture and in absence of PTPβ. The representative immunoblots for dephosphorylation and controls are shown in panels A and B, respectively, and a quantitative representation of normalized phosphorylation levels at different time points after addition of PTPβ is shown in panel C. The data were fitted to a one-phase exponential decay for TPR-MET (■) and cytoMET (△) using GraphPad Prism. Each point in panel B represents three independent experiments carried out in duplicate at a fixed concentration. The insets in panel C represent the data at early times, and the slope of the line depicted in the insets represents the initial velocity of dephosphorylation for cytoMET (△) and TPR-MET (■) at 1 μM. Data were fit to Michealis−Menten curves (D). The fits for cytoMET and TPR-MET are indicated by solid lines and dotted lines, respectively, in panels C and D.

phate into either TPR-MET or cytoMET, indicating both kinases were completely phosphorylated (data not shown). No dephosphorylation was observed over time in stored solutions of purified kinases prior to the dephosphorylation assay (data not shown).

Differential Dephosphorylation of Oligomeric TPR-MET and Monomeric CytoMET by PTPβ. To test the effects of oligomerization on dephosphorylation, we compared the overall dephosphorylation rates of equimolar quantities of phosphorylated cytoMET and TPR-MET. The rate and extent of dephosphorylation in each protein were examined using the commercially available recombinant PTPβ catalytic domain (~65 kDa). This phosphatase belongs to the receptor-like protein tyrosine phosphatase (RPTP) subfamily, which includes DEP-1, a reported physiological phosphatase for c-MET (*28*). Approximately 50% overall sequence identity existed between PTPβ and DEP-1, and ~60% sequence identity and 80% sequence similarity were found between their catalytic domains (data not shown).

Equimolar amounts (1 μM) of fully phosphorylated TPR-MET and cytoMET were separately incubated with PTPβ. Preliminary studies showed that TPR-MET consistently required more phosphatase than cytoMET to achieve comparable dephosphorylation between the two proteins. No significant dephosphorylation of TPR-MET was observed at low PTPβ concentrations. No dephosphorylation was observed for either TPR-MET or cytoMET when PTPβ was not included in the reaction (Figure 3B). Aliquots were removed from each phosphatase reaction mixture at fixed times, and the reactions were quenched by addition of SDS−PAGE buffer. The degree of tyrosine phosphorylation in each reaction aliquot was examined by phosphotyrosine immunoblotting (Figure 3A). All immunoblotting experiments were performed within the linear dynamic range of the antibody signal and the exposure time. Both TPR-MET and cytoMET were dephosphorylated during the 120 min reaction period that was examined, within which cytoMET was dephosphorylated more rapidly and to a greater extent than TPR-MET (Figure 3A). Although the comprehensive studies discussed in this paper utilized PTPβ for reasons cited above, preliminary experiments with other commercially available phosphatases (PTP1B and CIAP) yielded similar results, with cytoMET clearly dephosphorylated more rapidly and to a greater extent than TPR-MET (Figure 4). No significant differences in the dephosphorylation reactions were observed when the reactions described above were performed with the addition of 1 μM generic kinase inhibitor staurosporine in the dephosphorylation buffers (Figure 3B). Previous studies have shown that staurosporine was a potent inhibitor of kinase activites of purified cytoMET (K_I = 0.15 nM) and TPR-MET (K_I = 0.19 nM) (*21*). Thus, this control eliminated the possibility that the observed differences in global

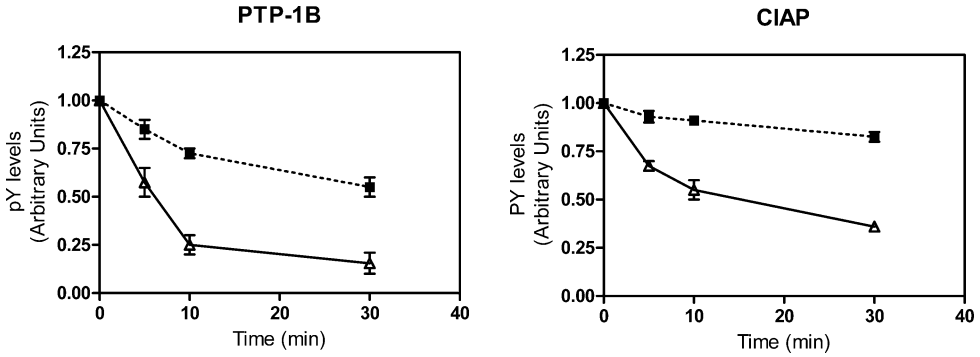

FIGURE 4: PTP1B and CIAP induced dephosphorylation in cytoMET and TPR-MET. Purified phosphorylated protein (1 μM) was incubated in phosphatase buffer with PTPIB and alkaline phosphatase, and aliquots were removed at the indicated times. The assay was performed as described for global dephosphorylation. The quantitative representation of normalized phosphorylation levels at different time points after addition of PTP1B and alkaline phosphatase is shown. The data for TPR-MET (■) and cytoMET (△) represent two independent experiments carried out in duplicate at a fixed concentration.

Table 1: Dephosphorylation Velocities of TPR-MET and CytoMET[a]

sites	V_0(cytoMET) (unit/min)	V_0(TPR-MET) (unit/min)	V_0(cytoMET)/ V_0(TPR-MET)
all	0.0983 ± 0.022	0.0194 ± 0.002	~ 5 ($p = 0.0053$)
$Y^{1234,1235}$	0.0902 ± 0.002	0.038 ± 0.012	~ 2.5 ($p = 0.0074$)
Y^{1349}	0.110 ± 0.021	0.017 ± 0.01	~ 7 ($p = 0.0003$)
Y^{1365}	0.095 ± 0.036	0.014 ± 0.011	~ 6.5 ($p = 0.0004$)

[a] Dephosphorylation of equimolar quantities of similarly phosphorylated cytoMET and TPR-MET was analyzed as described in Experimental Procedures. The V_0 values represent the $V_0 \pm$ the standard error for unweighted nonlinear least-square regression analyses of the data from Figure 2. Two-tailed p values were calculated using paired t tests.

dephosphorylation rates and phosphotyrosine levels were due to the differences in re-autophosphorylation rates of the purified proteins that were induced by possible residual ATP in the storage buffers.

The global dephosphorylation reaction data for each receptor were fit to exponential decay equations. Analyses of the curves showed that cytoMET dephosphorylation occurred rapidly, and was essentially complete within 30 min (Figure 3C). Under similar reaction conditions, the dephosphorylation rate of TPR-MET was substantially slower. Significant differences in the extent of dephosphorylation were also observed between the monomeric and dimeric form of the MET receptor. Although the global dephosphorylation reaction kinetics were fit to one-phase exponential decay models (Figure 3C) with an excellent goodness of fit obtained for both reactions ($R^2 > 0.9$), the reaction times were very long, which could result in the potential loss of PTPβ activity. If this occurred, it might adversely affect the accuracy of our quantitative exponential decay analysis and comparisons based on this analysis. Thus, quantitative comparisons between the two oligomeric states of the MET receptor relied on initial rates of dephosphorylation measured within time intervals where no loss of PTPβ activity was observed (data not shown). The slope of the lines plotted in the insets of Figure 3C provided initial dephosphorylation rates for the monomeric and dimeric receptor; the dephosphorylation rate of dimeric TPR-MET was ~5-fold slower than the dephosphorylation rate of its monomeric counterpart, cytoMET (Figure 3C and Table 1). Dephosphorylation rates calculated from parameters derived from exponential curves for data between 0 and 120 min gave similar results, with a 6-fold difference in dephosphorylation rates calculated for cytoMET and TPR-MET (data not shown). To make certain that this difference in dephosphorylation rates was not dependent upon a singular receptor concentration, we performed dephosphorylation reactions at additional cytoMET and TPR-MET concentrations ultimately spanning a 100-fold concentration range for the receptors. The data at these concentrations were qualitatively similar to our findings at 1 μM receptor, consistently showing that TPR-MET was dephosphorylated slower than cytoMET (Figure 3D). There are six possible phosphorylated tyrosine sites in TPR-MET and cytoMET, corresponding to Y^{1231}, Y^{1234}, Y^{1235}, Y^{1349}, Y^{1356}, and Y^{1365} in c-MET (Figure 1). A fit to the global dephosphorylation data could indicate two equally possible scenarios: either the dephosphorylation rate at each phosphotyrosine site were independent of the phosphorylation state of the other sites, or different multiphase exponential functions corresponding to different site dephosphorylation rates were too close to one another for us to deconvolute the separate exponentials from our data. Detailed kinetic analyses with site-specific antibodies (described in the next section), more sensitive probes, or site-specific mutants would be expected to differentiate between these models.

Estimations of K_M and V_{MAX} of PTPβ for cytoMET and TPR-MET substrates were derived by fitting the velocity data at different receptor concentrations to the Michealis−Menten (M−M) equation (Figure 3D). The experimental data for cytoMET and TPR-MET fit the M−M equation with a goodness of fit R^2 of >0.97. Significantly, different K_M and V_{MAX} values were calculated for TPR-MET and cytoMET as PTPβ substrates; PTPβ had an ~7-fold greater K_M and an ~2-fold smaller V_{MAX} for TPR-MET compared to cytoMET (Table 2). Interestingly, the observed PTPβ K_M values measured with the MET substrates were comparable to the micromolar K_M values observed for PTPβ reacting with several phosphotyrosine peptide substrates (*29*). Coupling the low K_M and increased V_{MAX} yielded a 10-fold decreased substrate specificity of PTPβ for TPR-MET relative to cytoMET. On the basis of these experiments, we concluded that the dephosphorylation profiles of similarly phosphorylated TPR-MET and cytoMET differed significantly such that TPR-MET had a slower rate of dephosphorylation and lower V_{MAX}/K_M than cytoMET did.

Dephosphorylation Kinetics of the Activation Loop and Carboxy-Terminal Tyrosines. Wild-type c-MET contains

Table 2: Kinetic Data for PTPβ Using CytoMET and TPR-MET as Substrates[a]

	TPR-MET			cytoMET		
sites	K_M (μM)	V_{MAX} (unit/min)	V_{MAX}/K_M	K_M (μM)	V_{MAX} (unit/min)	V_{MAX}/K_M
all	6.184 ± 1.547	0.132 ± 0.024	0.021	1.219 ± 0.297	0.247 ± 0.016	0.20
$Y^{1234,1235}$	4.544 ± 1.442	0.202 ± 0.036	0.044	1.550 ± 0.5280	0.271 ± 0.026	0.17
Y^{1349}	5.172 ± 1.721	0.102 ± 0.010	0.019	*b*	*b*	
Y^{1365}	4.184 ± 1.470	0.093 ± 0.011	0.022	*b*	*b*	

[a] Dephosphorylation of cytoMET and TPR-MET was analyzed as described in Experimental Procedures. The values reported represent $V_{MAX} \pm$ the standard error and $K_M \pm$ the standard error for unweighted nonlinear least-square regression analyses of the data from Figures 2 and 3. Two-tailed *p* values were calculated using paired *t* tests. [b] Data did not fit the Michealis−Menten equation.

three phosphotyrosine sites within its activation loop (Y^{1230}, Y^{1234}, and Y^{1235}) and three phosphotyrosine sites within its carboxy-terminal tail (Y^{1349}, Y^{1356}, and Y^{1365}). These phosphorylation sites were present in both cytoMET and TPR-MET (Figure 1). Phosphorylation of activation loop tyrosines 1234 and 1235 has been shown to be important for the increased kinase activity of the receptor (*25*). Phosphorylation of carboxy-tail tyrosine 1349 and 1356 has been shown to be necessary for recruitment of downstream effector molecules Gab1 and Grb2, respectively (*22*). Although proteins that interact with phosphorylated tyrosine 1365 have not been identified, mutation analyses have indicated that this site was involved in morphogenesis (*30*). To probe the impact of oligomerization on the structural and functional properties of the activation loop and carboxy-tail subdomains, site-specific antibodies were used to compare dephosphorylation rates of specific phosphotyrosines in cytoMET and TPR-MET.

Purified cytoMET and TPR-MET were separately dephosphorylated with PTPβ under similar conditions that were used for the global dephosphorylation assay. The membranes were sequentially probed with anti-phospho $Y^{1234,1235}$, anti-phospho Y^{1365}, and anti-MET antibodies with the membranes extensively stripped between each primary antibody. CytoMET and TPR-MET showed clear differences in the intensity patterns of the antibody response from the activation loop and carboxy-tail regions (Figure 5A). Detailed comparative quantitative analysis of the digitized antibody signals showed cytoMET was dephosphorylated at a faster rate than TPR-MET on both its activation loop tyrosines $Y^{1234,1235}$ and its carboxy-tail tyrosine Y^{1365} (Figure 5B). The initial dephosphorylation rate for the activation loop calculated from the linear response region of the dephosphorylation reaction (inset of Figure 5B, left-hand panel) was ~2.5-fold larger for cytoMET than it was for TPR-MET (Table 1). The data for cytoMET and TPR-MET activation loop dephosphorylation were separately fit to one-phase exponential decay curves ($R^2 > 0.95$; Figure 5B, left-hand panel), and comparable differences in dephosphorylation rates for dimeric TPR-MET and monomeric cytoMET were independently calculated from these curve fits (data not shown). In contrast, the dephosphorylation rate of the carboxy-tail phosphotyrosine was ~6-fold slower in TPR-MET than in cytoMET based on initial dephosphorylation rates (Table 1 and Figure 5B, right-hand panel). The dephosphorylation data for the carboxy-tail Y^{1365} were fit to a two-phase exponential for cytoMET ($R^2 = 0.95$) and one-phase exponential for TPR-MET ($R^2 = 0.93$), and rate constants calculated from these fits gave an ~10-fold difference in the dephosphorylation rates for the carboxy-tail site (data not shown). Interestingly, the second exponential term of the cytoMET Y^{1365} dephosphorylation curve had a decay constant that was not significantly different from the decay constant calculated for the TPR-MET dephosphorylation exponential curve. The two-phase exponential observed for cytoMET carboxy-tail dephosphorylation could imply changes in the local conformational environment of Y^{1365} due to dephosphorylation at distant sites. The decreased slope and decay constant observed in the second phase (late reaction times) of the cytoMET dephosphorylation curve relative to the first phase (early reaction times) of the curve implied that the dephosphorylation rate of Y^{1365} slowed as additional cytoMET sites were dephosphorylated. The initial dephosphorylation rates and curves measured in cytoMET and TPR-MET for another carboxy-tail phosphotyrosine site, Y^{1349}, were very similar to those values measured for the carboxy-tail site Y^{1365}, and the dephosphorylation rate at Y^{1349} was ~7-fold slower in TPR-MET than in cytoMET (Table 1). Similar qualitative differences in the activation loop and carboxy-tail phosphotyrosine dephosphorylation rates of cytoMET and TPR-MET were measured at several receptor concentrations covering a 100-fold receptor concentration range (Figure 5C). The initial velocities computed from the straight line slopes (insets, Figure 5B) at different receptor concentrations fit the M−M equation well for cytoMET and TPR-MET activation loop phosphotyrosine dephosphorylation (Figure 5C, left-hand panel). PTPβ exhibited an ~3-fold difference in the K_M and a non-statistically significant difference in V_{MAX} for activation loop dephosphorylation between the different oligomeric states of the receptor. The M−M parameter comparison between cytoMET and TPR-MET carboxy-tail phosphotyrosine dephosphorylation was not made since the cytoMET data did not fit the M−M equation well ($R^2 = 0.85$). However, dephosphorylation rates at all substrate concentrations that were examined clearly showed dephosphorylation was significantly faster for the carboxy-tail tyrosines in cytoMET than in TPR-MET (Figure 5C, right-hand panel, and Table 2).

Our kinetic analyses consistently showed that TPR-MET activation loop and carboxy-tail phosphotyrosines had reduced susceptibility relative to cytoMET to phosphatase-catalyzed dephosphorylation. Interestingly, while the activation loop dephosphorylation rates between monomeric cytoMET and dimeric TPR-MET differed by at least 3-fold, there was an even greater ~7-fold difference in the carboxy-tail dephosphorylation rates between these two receptor states. This implied that oligomerization impacted the two domains of the receptors to different extents.

Pervanadate-Induced Phosphorylation of Wild-Type Unligated c-MET in Intact Cells. Our studies using the well-defined TPR-MET/cytoMET system showed that cytoMET functioned as a better phosphatase substrate than TPR-MET.

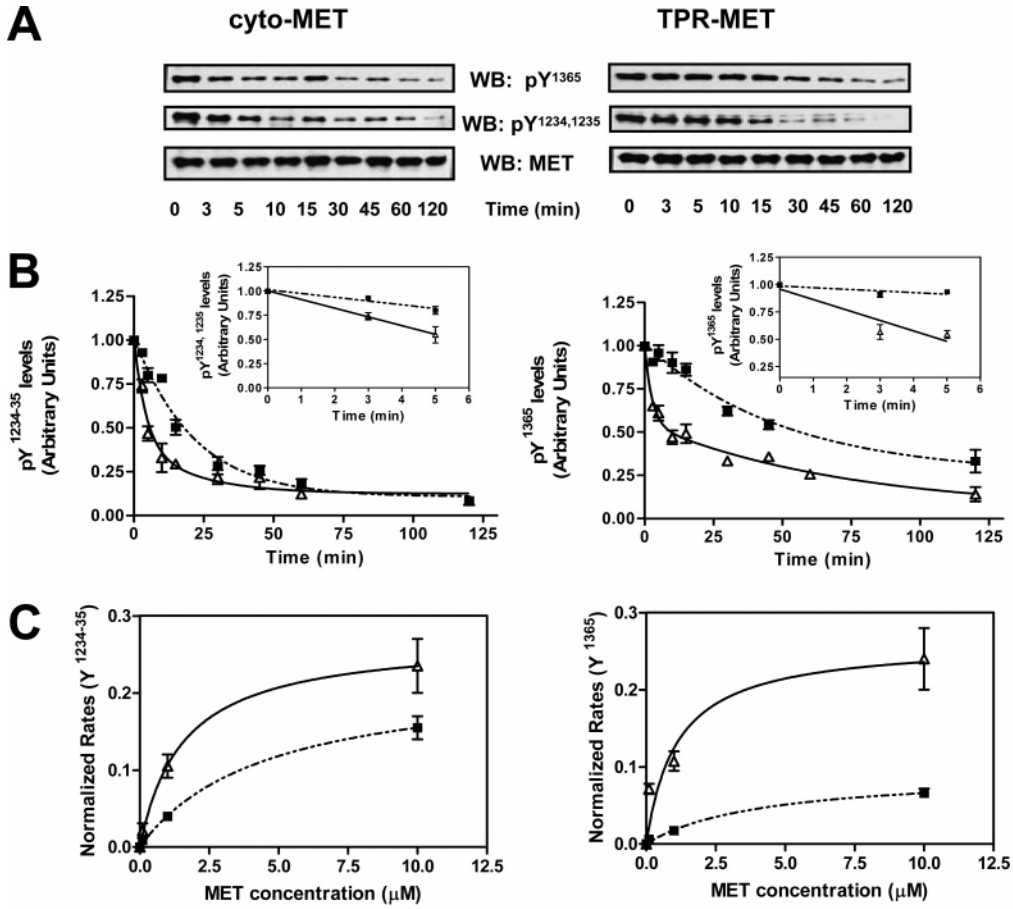

FIGURE 5: Site-specific dephosphorylation in cytoMET and TPR-MET. Purified phosphorylated proteins (1 μM) were incubated in phosphatase buffer with PTPβ, and aliquots were removed at the indicated times. The proteins were separated on polyacrylamide gels, transferred to a PVDF membrane, and probed with different site-specific antibodies. The blots were stripped and reprobed with anti-MET antibody. The representative immunoblots for the $Y^{1234,1235}$ dephosphorylation (left) and Y^{1365} dephosphorylation (right) are shown in panel A, and quantitative representation of normalized phosphorylation levels at different time points after addition of PTPβ is shown in panel B. The data were fitted to one-phase [$Y^{1234,1235}$ cytoMET (△), $Y^{1234,1235}$ TPR-MET (■), and Y^{1365} TPR-MET (■)] or two-phase [Y^{1365}, cytoMET (△)] exponential decay using GraphPad Prism. The insets in panel B represent the data at the early time points, and the slope of the line depicted in the insets represents the initial velocity of dephosphorylation for cytoMET (△) and TPR-MET (■). Each point in panel B represents three independent experiments carried out in duplicate, and error bars represent the standard error. Data were fit to Michealis−Menten curves (C). The fits for cytoMET and TPR-MET are indicated by solid lines and dotted lines, respectively, in panels B and C.

Increased sensitivity to dephosphorylation in cytoMET compared to TPR-MET implied that phosphatase might efficiently dephosphorylate monomeric unstimulated c-MET on the cell surface, thereby providing an additional mechanism of regulating receptor signaling. Since direct comparison of dephosphorylation rates between monomeric and dimeric receptor states in intact cells was problematic, due in part to difficulties in determining receptor oligomerization levels and obtaining phosphorylated monomeric receptor, the presence of saturating ATP concentrations in the cellular environment, and differential effects of adapter molecules, we monitored phosphorylation of unstimulated c-MET upon PTP inhibition. This process could be clearly followed, and served as a probe for phosphatase activity directed against monomeric c-MET. Although PTP inhibition by pervanadate has resulted in PDGFR and IR phosphorylation (*17*, *18*), it was unknown whether analogous receptor phosphorylation would occur for c-MET. Furthermore, the sites that were phosphorylated upon PTP inhibition in IR and PDGFR were unknown. We hypothesized that c-MET will be phosphorylated on all functionally important tyrosines upon PTP inhibition.

Serum-starved confluent Vero cells were treated with pervanadate, a potent phosphatase inhibitor, as described for related experiments with IR and PDGFR (*17*, *18*). The cells were lysed at various times post-treatment, and c-MET was immunoprecipitated and immunoblotted with phosphotyrosine antibodies. The blots were stripped and reprobed with site-specific antibodies to monitor specific phosphotyrosine sites. Although similar amounts of c-MET were immunoprecipitated at each time post-treatment, a time-dependent increase in c-MET phosphorylation levels was observed upon pervanadate stimulation (Figure 6). Immunoblots with phosphotyrosine antibody showed a buildup of phosphorylated c-MET occurred within 2 min post-treatment and phosphotyrosine levels peaked at ∼30 min post-treatment (Figure 6A). Reprobing the blot with anti-phospho Y^{1365}, anti-phospho Y^{1349}, and anti-phospho $Y^{1234,1235}$ antibodies showed c-MET phosphorylation on all examined c-MET functionally important sites occurred within 5 min of pervanadate treatment. Notably, the carboxy-tail phosphotyrosine sites clearly showed a delay in phosphorylation relative to the activation loop phosphotyrosine sites (Figure 6B). Interestingly, the amount of both total c-MET and phosphorylated c-MET

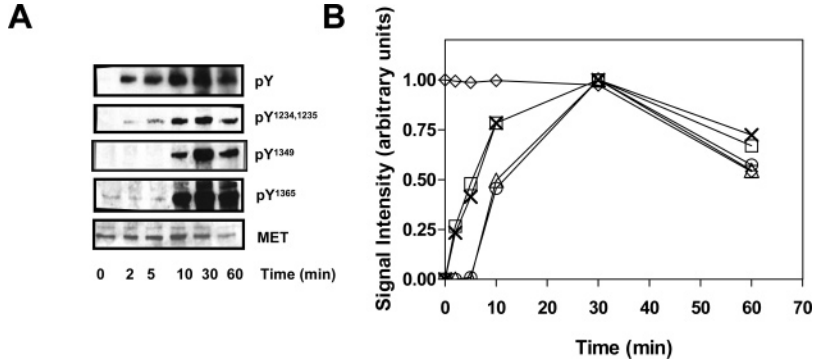

FIGURE 6: Effects of phosphatase inhibitor on c-MET monomer phosphorylation. Vero cells were grown to near confluency and serum starved for 12−24 h. Cells were treated with pervanadate and lysed at the indicated times. c-MET was immunoprecipitated using antibody to the extracellular region (DO-24). The receptor was then separated by SDS−PAGE and transferred to a PVDF membrane. The membrane was probed with phosphotyrosine antibody and stripped and reprobed with different c-MET phospho-site-specific antibodies. The blots were stripped and reprobed with anti-MET antibody. The representative immunoblots are shown in panel A, and a quantitative representation of normalized signal intensities is depicted in panel B for $Y^{1234,1235}$ (×), Y^{1365} (△), Y^{1349} (○), PY (□), and MET (◇). Each point in panel B represents three independent experiments carried out in duplicate. The error bars representing the standard error are smaller than the symbol size and hence not included in the figure for clarity.

recovered from cells decreased ~30 min post-treatment, implying c-MET degradation was likely occurring at this time. Cells stimulated with sodium orthovanadate also triggered a buildup of phosphorylated c-MET, although to a lesser extent than that observed with the more potent PTP inhibitor pervanadate (data not shown). No phosphorylation of unstimulated c-MET occurred when cells were treated with buffer lacking PTP inhibitor. These results conclusively showed that rapid phosphorylation of c-MET functionally important tyrosines occurred when PTP activity was blocked, thus implying that PTPs play an important role in eliminating phosphorylation of unstimulated c-MET.

DISCUSSION

The importance of c-MET signaling is highlighted by its function in angiogenesis, placental and liver development, B-cell differentiation, embryogenesis, and dysregulation in multiple neoplastic disorders (*31*). The molecular mechanism regulating c-MET activation and signaling are not completely understood. The activation process of RTKs such as c-MET has typically been described as a series of sequential steps involving cognate ligand binding, receptor dimerization, receptor autophosphorylation, substrate recruitment and phosphorylation, and eventual downregulation of the receptor activity mediated by ligand dissociation, dephosphorylation, and/or degradation. To provide a more detailed and quantitative model of receptor activation, previous studies from our laboratory examined how oligomerization modulated receptor kinase activity (*20*, *21*). These studies used phosphorylated TPR-MET and cytoMET, well-defined functional surrogates for signaling-competent dimeric and inactive monomeric c-MET, and showed that the oligomeric state of the receptor markedly changed its kinetic and thermodynamic properties. In this paper, we sought to extend our understanding of receptor activation and regulation by investigating the impact of oligomerization on c-MET dephosphorylation.

Consistent with preliminary dephosphorylation studies on PDGFR (*19*), dimeric TPR-MET displayed increased resistance to dephosphorylation as compared to monomeric cytoMET. Significantly, the oligomerization-dependent changes in dephosphorylation rates were different for the activation loop and carboxy-terminal subdomains of the receptor. Dimerization of the receptor reduced the susceptibility of its activation loop and carboxy-tail phosphotyrosines to dephosphorylation by ~3- and ~7-fold, respectively, at 1 μM MET. Two possible explanations are consistent with these observations; namely, dimerization induces conformational changes in the MET receptor that make it less susceptible to dephosphorylation relative to the monomeric MET receptor, or dimerization produces steric effects that "shield" the phosphotyrosine sites from phosphatases. The differences in K_M values for overall phosphorylation could support the hypotheses stated above; however, differences in V_{MAX} imply a possible structural reorganization of the substrate site as opposed to a mere "shielding effect". In addition, the switch between non-Michealis−Menten and Michealis−Menten kinetics observed for the cytoMET and TPR-MET carboxy-tail phosphotyrosine supports a model of structural reorganization occurring during receptor oligomerization. The differences between cytoMET and TPR-MET in dephosphorylation rates for the activation loop as well as carboxy-tail phosphotyrosines suggest that upon oligomerization conformational changes occur in several domains within the receptor. The precise understanding of the nature of these dimerization-induced conformational and/or possible dynamics changes awaits further studies. The different reaction kinetics shown by PTPβ toward protein substrates in different oligomerization states indicate that PTPβ-catalyzed dephosphorylation is more complex for protein substrates than for phosphotyrosylpeptide substrates.

Classically, it was believed that the sole role of ligand-induced receptor oligomerization was to autophosphorylate the receptor's activation loop, which in turn was believed to be necessary for activation of the receptor's kinase function. In vitro studies using isolated kinase domains (*18*, *24*) and ex vivo studies using phosphatase inhibitor have shown conclusively that monomeric receptors can be rapidly phosphorylated on tyrosine residues involved in intracellular signal propagation (*17*, *18*). Thus, it is clear that ligand-induced receptor oligomerization is not necessary for kinase activity.

Alternatively, our work and that of others (*24*, *32*) suggest that RTK oligomerization is necessary to rapidly switch the receptor between distinct signaling-incompetent and signal-

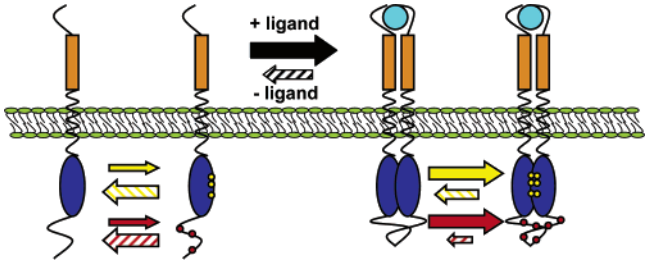

FIGURE 7: Model of receptor activation upon ligand binding. In the absence of any ligand, the monomeric receptor resides on the cell membrane tightly regulated by the action of phosphatases. When ligand binds, the receptors dimerize and the system shifts to a different equilibrium state. Accumulation of the phosphorylated receptor occurs due to the synergistic combination of increased kinase activity, resulting from oligomerization-dependent catalytic changes and activation loop phosphorylation and decreased dephosphorylation rates associated with the dimeric species. The equilibrium established by the autophosphorylation (black, yellow, and red arrows) and dephosphorylation (gray arrows) reactions for the activation loop (orange circles) and carboxy-terminal tyrosines (red circles) is depicted for monomeric unstimulated and ligand-stimulated receptors on the cell surface.

ing-competent states. In this model, a RTK is in a signaling-competent state when it is phosphorylated at specific tyrosine residues and capable of binding and activating immediate downstream effectors (e.g., PI3K, Gab1, and Grb2). The receptor is in a signaling-incompetent state when it is dephosphorylated and unable to bind and activate immediate downstream effectors. Neither functional state is restricted to a particular oligomeric state; it is possible to observe monomeric signaling-competent states and oligomeric signaling-incompetent states. As shown in our previous studies, oligomerization modifies the thermodynamic and kinetic properties of the MET kinase domain such that dimeric phosphorylated MET more efficiently phosphorylates substrate molecules than the monomeric phosphorylated MET (*20*, *21*). It is likely, though not yet proven, that oligomerization causes similar changes in unphosphorylated MET kinase activity. Several studies have also shown that receptor autophosphorylation occurs more rapidly for oligomeric receptors than for monomeric receptors (*12*, *33*; S. J. Watowich, unpublished data), although kinetic parameters associated with monomer and dimer receptor autophosphorylation have only been quantitatively measured for IR (*33*). Kinase activity is additionally regulated by phosphorylation levels, in particular, the phosphorylation state of tyrosines within the receptor activation loop. Thus, both receptor phosphorylation and receptor oligomeric states clearly modulate receptor kinase activity. Moreover, the extent of receptor phosphorylation is regulated by competing autophosphorylation and dephosphorylation reactions which in turn are modulated by the receptor oligomeric state. Thus, receptor oligomerization can either directly modulate kinase activity or indirectly modulate kinase activity by modulating autophosphorylation and dephosphorylation rates which impact receptor phosphorylation levels and in turn affect kinase activity (Figure 7). The interdependency between phosphorylation state, oligomerization state, and kinase activity enables receptor oligomerization to amplify the sharp separation between signaling-competent and signaling-incompetent states.

A mechanistic model of receptor signaling that incorporates the multiple regulatory effects of receptor oligomerization is shown in Figure 7. In the absence of ligand stimulation, monomeric receptors reside at the cell membrane. The autophosphorylation of the unstimulated monomeric receptor is balanced by cellular phosphatases present either on the cell surface on in the cytoplasm of the cells such that the monomeric receptor remains phosphorylated. Tight regulation of the monomeric receptor by phosphatases could function to prevent nonspecific signaling. Extracellular ligand stimulation causes receptor dimerization, which changes the equilibrium state of the system. Accumulation of the phosphorylated dimeric receptor results from the synergistic combination of properties associated with this dimeric state, i.e., an increased kinase activity (resulting from oligomerization-dependent catalytic changes and activation loop phosphorylation) and decreased susceptibility to dephosphorylation. These properties produce the signaling-competent state observed for the dimeric receptor, which is capable of producing specific and sustained signaling responses.

The results presented in this paper directly demonstrate for the first time the effects of oligomerization in modifying the dephosphorylation rates of the c-MET substrate. We have shown that phosphorylated TPR-MET is dephosphorylated at a slower rate than phosphorylated cytoMET. Site-specific dephosphorylation measurements corroborated the overall dephosphorylation data, with TPR-MET displaying resistance to dephosphorylation on its activation loop and increased resistance on the carboxy-tail phosphotyrosines required for signaling. The implications of these findings are particularly important in furthering our understanding of the activation mechanism of RTKs.

ACKNOWLEDGMENT

We thank Dr. L. Elferink and Dr. J. Hays for helpful discussions and Dr. M. Park for providing the *tpr-met* clone. We thank Dr. J. Papaconstantinou for the use of imaging equipment and software for our Western blot quantifications. We are grateful to Dr. George Vande Woude (Van Andel Research Institute, Grand Rapids, MI) for critical reading of the manuscript and helpful discussions.

REFERENCES

1. Hubbard, S. R., and Till, J. H. (2000) Protein tyrosine kinase structure and function, *Annu. Rev. Biochem. 69*, 373−398.
2. Ullrich, A., and Schlessinger, J. (1990) Signal transduction by receptors with tyrosine kinase activity, *Cell 61*, 203−212.
3. Schlessinger, J. (2000) Cell signaling by receptor tyrosine kinases, *Cell 103*, 211−225.
4. Schlessinger, J., and Ullrich, A. (1992) Growth factor signaling by receptor tyrosine kinases, *Neuron 9*, 383−391.
5. Wiesmann, C., Fuh, G., Christinger, H. W., Eigenbrot, C., Wells, J. A., and de Vos, A. M. (1997) Crystal structure at 1.7 Å resolution of VEGF in complex with domain 2 of the Flt-1 receptor, *Cell 91*, 695−704.
6. Schlessinger, J., Plotnikov, A. N., Ibrahimi, O. A., Eliseenkova, A. V., Yeh, B. K., Yayon, A., Linhardt, R. J., and Mohammadi, M. (2000) Crystal structure of a ternary FGF−FGFR−heparin complex reveals a dual role for heparin in FGFR binding and dimerization, *Mol. Cell 6*, 743−750.
7. Ogiso, H., Ishitani, R., Nureki, O., Fukai, S., Yamanaka, M., Kim, J. H., Saito, K., Sakamoto, A., Inoue, M., Shirouzu, M., and Yokoyama, S. (2002) Crystal structure of the complex of human epidermal growth factor and receptor extracellular domains, *Cell 110*, 775−787.

8. Mohammadi, M., Schlessinger, J., and Hubbard, S. R. (1996) Structure of the FGF receptor tyrosine kinase domain reveals a novel autoinhibitory mechanism, *Cell 86*, 577−587.
9. Mohammadi, M., Froum, S., Hamby, J. M., Schroeder, M. C., Panek, R. L., Lu, G. H., Eliseenkova, A. V., Green, D., Schlessinger, J., and Hubbard, S. R. (1998) Crystal structure of an angiogenesis inhibitor bound to the FGF receptor tyrosine kinase domain, *EMBO J. 17*, 5896−5904.
10. Hubbard, S. R., Wei, L., Ellis, L., and Hendrickson, W. A. (1994) Crystal structure of the tyrosine kinase domain of the human insulin receptor, *Nature 372*, 746−754.
11. Hubbard, S. R. (1997) Crystal structure of the activated insulin receptor tyrosine kinase in complex with peptide substrate and ATP analog, *EMBO J. 16*, 5572−5581.
12. Posner, I., Engel, M., and Levitzki, A. (1992) Kinetic model of the epidermal growth factor (EGF) receptor tyrosine kinase and a possible mechanism of its activation by EGF, *J. Biol. Chem. 267*, 20638−20647.
13. Cann, A. D., and Kohanski, R. A. (1997) Cis-autophosphorylation of juxtamembrane tyrosines in the insulin receptor kinase domain, *Biochemistry 36*, 7681−7689.
14. Kohanski, R. A. (1993) Insulin receptor autophosphorylation. I. Autophosphorylation kinetics of the native receptor and its cytoplasmic kinase domain, *Biochemistry 32*, 5766−5772.
15. Kohanski, R. A. (1993) Insulin receptor autophosphorylation. II. Determination of autophosphorylation sites by chemical sequence analysis and identification of the juxtamembrane sites, *Biochemistry 32*, 5773−5780.
16. Murray, B. W., Padrique, E. S., Pinko, C., and McTigue, M. A. (2001) Mechanistic effects of autophosphorylation on receptor tyrosine kinase catalysis: Enzymatic characterization of Tie2 and phospho-Tie2, *Biochemistry 40*, 10243−10253.
17. Posner, B. I., Faure, R., Burgess, J. W., Bevan, A. P., Lachance, D., Zhang-Sun, G., Fantus, I. G., Ng, J. B., Hall, D. A., Lum, B. S., and Shaver, A. (1994) Peroxovanadium compounds. A new class of potent phosphotyrosine phosphatase inhibitors which are insulin mimetics, *J. Biol. Chem. 269*, 4596−4604.
18. Baxter, R. M., Secrist, J. P., Vaillancourt, R. R., and Kazlauskas, A. (1998) Full activation of the platelet-derived growth factor β-receptor kinase involves multiple events, *J. Biol. Chem. 273*, 17050−17055.
19. Shimizu, A., Persson, C., Heldin, C. H., and Ostman, A. (2001) Ligand stimulation reduces platelet-derived growth factor β-receptor susceptibility to tyrosine dephosphorylation, *J. Biol. Chem. 276*, 27749−27752.
20. Hays, J. L., and Watowich, S. J. (2004) Oligomerization dependent changes in the thermodynamic properties of the TPR-MET receptor tyrosine kinase, *Biochemistry 43*, 10570−10578.
21. Hays, J. L., and Watowich, S. J. (2003) Oligomerization-induced modulation of TPR-MET tyrosine kinase, *J. Biol. Chem. 278*, 27456−27465.
22. Birchmeier, C., Birchmeier, W., Gherardi, E., and Vande Woude, G. F. (2003) Met, metastasis, motility and more, *Nat. Rev. Mol. Cell Biol. 4*, 915−925.
23. Trusolino, L., and Comoglio, P. M. (2002) Scatter-factor and semaphorin receptors: Cell signaling for invasive growth, *Nat. Rev. Cancer 4*, 289−300.
24. Rodrigues, G. A., and Park, M. (1993) Dimerization mediated through a leucine zipper activates the oncogenic potential of the met receptor tyrosine kinase, *Mol. Cell. Biol. 13*, 6711−6722.
25. Rodrigues, G. A., and Park, M. (1994) Autophosphorylation modulates the kinase activity and oncogenic potential of the Met receptor tyrosine kinase, *Oncogene 9*, 2019−2027.
26. Kulas, D. T., Goldstein, B. J., and Mooney, R. A. (1996) The transmembrane protein-tyrosine phosphatase LAR modulates signaling by multiple receptor tyrosine kinases, *J. Biol. Chem. 271*, 748−754.
27. Villa-Moruzzi, E., Puntoni, F., Bardelli, A., Vigna, E., De Rosa, S., and Comoglio, P. M. (1998) Protein tyrosine phosphatase PTP-S binds to the juxtamembrane region of the hepatocyte growth factor receptor Met, *Biochem. J. 336*, 235−239.
28. Palka, H. L., Park, M., and Tonks, N. K. (2003) Hepatocyte growth factor receptor tyrosine kinase Met is a substrate of the receptor protein-tyrosine phosphatase DEP-1, *J. Biol. Chem. 278*, 5728−5735.
29. Cho, H., Krishnaraj, R., Itoh, M., Kitas, E., Bannwarth, W., Saito, H., and Walsh, C. T. (1993) Substrate specificities of catalytic fragments of protein tyrosine phosphatases (HPTPb, LAR, and CD45) towards phosphotyrosylpeptide substrates and thiophosphotyrosylated peptides as inhibitors, *Protein Sci. 2*, 977−984.
30. Weidner, K. M., Sachs, M., Reithmacher, D., and Birchmeier, W. (1995) Mutation of juxtamembrane tyrosine residue 1001 suppresses loss-of-function mutations of the met receptor in epithelial cells, *Proc. Natl. Acad. Sci. U.S.A. 92*, 2597−2601.
31. van der Voort, R., Taher, T. E., Derksen, P. W., Spaargaren, M., van der Neut, R., and Pals, S. T. (2000) The hepatocyte growth factor/Met pathway in development, tumorigenesis, and B-cell differentiation, *Adv. Cancer Res. 79*, 39−90.
32. Hubbard, S. R., Mohammadi, M., and Schlessinger, J. (1998) Autoregulatory mechanisms of protein-tyrosine kinases, *J. Biol. Chem. 273*, 11987−11990.
33. Baer, K., Al-Hasani, H., Parvaresch, S., Corona, T., Rufer, A., Nolle, V., Bergschneider, E., and Klein, H. W. (2001) Dimerization-induced activation of soluble insulin/IGF-1 receptor kinases: An alternative mechanism of activation, *Biochemistry 40*, 14268−14278.

BI050855U